

# Model Predictive Control with Reference Learning for Soft Robotic Intracranial Pressure Waveform Modulation

Fabian Flürenbrock, Yanick Büchel, Johannes Köhler, Marianne Schmid Daners, and Melanie N. Zeilinger

**Abstract**—This paper introduces a learning-based control framework for a soft robotic actuator system designed to modulate intracranial pressure (ICP) waveforms, which is essential for studying cerebrospinal fluid dynamics and pathological processes underlying neurological disorders. A two-layer framework is proposed to safely achieve a desired ICP waveform modulation. First, a model predictive controller (MPC) with a disturbance observer is used for offset-free tracking of the system’s motor position reference trajectory under safety constraints. Second, to address the unknown nonlinear dependence of the ICP on the motor position, we employ a Bayesian optimization (BO) algorithm used for online learning of a motor position reference trajectory that yields the desired ICP modulation. The framework is experimentally validated using a test bench with a brain phantom that replicates realistic ICP dynamics *in vitro*. Compared to a previously employed proportional-integral-derivative controller, the MPC reduces mean and maximum motor position reference tracking errors by 83 % and 73 %, respectively. In less than 20 iterations, the BO algorithm learns a motor position reference trajectory that yields an ICP waveform with the desired mean and amplitude.

## I. INTRODUCTION

The regulation of pressure is a fundamental requirement in many biological systems. Specifically, intracranial pressure (ICP) plays a crucial role in the brain and central nervous system. It affects cerebrospinal fluid (CSF) dynamics and also directly impacts neurological health. Hydrocephalus is a medical condition characterized by disturbed CSF dynamics and an excessive accumulation of CSF within the cerebral ventricles [1], [2], commonly treated using shunt systems [3]. While mean ICP is an important clinical marker for this condition, the pulsatile components of the ICP waveform have gained increasing attention in research as these may reflect and contribute to the underlying pathological processes [4], [5]. Monitoring, understanding, and controlling the ICP waveform is therefore essential for advancing the study and therapy of neurological disorders such as hydrocephalus.

Various research groups have developed robotic systems to perform active modulation of the ICP waveform in animal studies [6–16]. While the respective research objectives slightly differ among them, the developed systems are commonly based on motorized pumps, which cyclically inflate and deflate a balloon that is placed within a location of the CSF system such as the cerebral ventricles. As the cardiac cycle is the primary driver of the pulsatile ICP waveform [17],

This work was supported by the Swiss National Science Foundation (Grant 315230 184913) and the NCCR Automation (51NF40 180545). All authors are with the Institute for Dynamic Systems and Control at ETH Zurich, Switzerland. E-mail: {ffluerenb, ybuechel, jkoehle, marischm, mzeilinger}@ethz.ch

inflation and deflation of the balloon are gated to the electrocardiogram (ECG) and performed during the systolic phase of the heartbeat, during which ventricular blood ejection raises arterial pressure and drives ICP pulsation. The control of these motorized pump systems is typically implemented using open-loop or proportional–integral–derivative (PID) controllers. However, since the exact influence of the motor position on the ICP is unknown, achieving the desired ICP waveform modulation with these control approaches requires *time-consuming and error-prone hand-tuning* of the motor’s reference trajectory and control parameters. An additional challenge is that the safety of the aspired *in vivo* intervention must be ensured during the whole tuning process and throughout the subsequent deployment. Incorrect inflation and deflation of the implanted balloon can not only cause undesired baseline shifts in the ICP but also lead to pathological levels of ICP or even mechanical failure of the balloon. Accurate and offset-free tracking of the motor position reference trajectory and the integration of safety constraints are thus required. Since the systolic phase of the heartbeat is only about 350 ms long [18], this task poses a challenging control problem.

**Contribution:** This paper introduces a learning-based control framework to improve both the safety and performance of a soft robotic actuator system [16] used for ICP waveform modulation in hydrocephalus research. To this end, three contributions are presented:

- 1) A model predictive controller (MPC) [19] for reference tracking is designed and augmented with a disturbance observer that exploits the periodic operation of the system. The MPC scheme improves system performance through offset-free tracking of the motor position reference trajectory and enhances safety through explicit integration of the system’s state and input constraints.
- 2) A Bayesian optimization (BO) [20] algorithm for data-efficient and automated MPC reference learning is designed. The BO algorithm improves system performance by iteratively tuning the parameterized motor position reference trajectory of the MPC during runtime, thereby learning the optimal reference trajectory that results in the desired ICP waveform modulation.
- 3) The introduced learning-based control framework is deployed on the soft robotic actuator system [16], and the active ICP waveform modulation experimentally investigated using a mechatronic test bench that features a brain phantom capable of replicating physiological ICP waveforms *in vitro* [21].

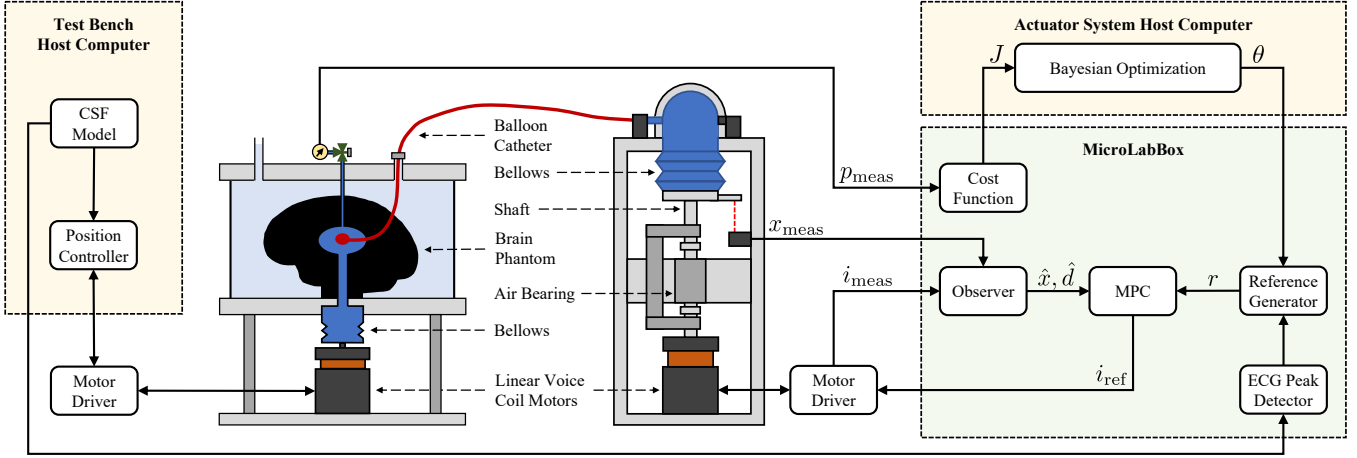


Fig. 1. Schematic overview of the experimental hardware setup. The soft robotic actuator system has been developed in [16] and is used for intracranial pressure (ICP) modulation. The mechatronic test bench has been developed in [21] and is used for the physical replication of ICP waveforms. The balloon catheter of the soft robotic actuator system is inserted into the brain phantom of the test bench to enable ICP waveform modulation. The pressure measurements of the brain phantom and the electrocardiogram (ECG) of the cerebrospinal fluid (CSF) model used for simulating physiological ICP waveforms are fed back to the soft robotic actuator system.

*Outline:* In Section II, we abstract the problem considered in this work into a mathematical description and highlight the key technical difficulties. In Section III, we provide a general methodology to address the considered problem based on an MPC formulation for reference tracking and a BO algorithm for reference learning. In Section IV, we discuss the deployment and experimental validation of the methodology on hardware. Section V concludes the paper.

## II. PROBLEM FORMULATION

The experimental hardware setup of this work, composed of the soft robotic actuator system [16] and the mechatronic test bench [21], is sketched in Figure 1. To describe the soft robotic actuator system, the following discrete-time linear time-invariant system is considered

$$x(k+1) = Ax(k) + Bu(k) + B_d d(k), \quad (1a)$$

$$y(k) = Cx(k) + C_d d(k), \quad (1b)$$

where  $k \in \mathbb{N}$  denotes the discrete time step, the system state  $x \in \mathbb{R}^2$  consists of the motor position and velocity, the input  $u \in \mathbb{R}$  is the applied motor current, the output  $y \in \mathbb{R}$  is the measured motor position, and the additive disturbance  $d \in \mathbb{R}$  captures all unmodeled effects. We consider polytopic state and input constraints that are denoted as  $\mathbb{X} \subset \mathbb{R}^2$  and  $\mathbb{U} \subset \mathbb{R}$ , respectively. We assume that the system matrix  $A$  and input matrix  $B$  are approximately known through system identification. We further consider a reference  $r \in \mathbb{R}$  that is to be tracked by the system output. The shape of the reference trajectory for a full inflation and deflation cycle of the balloon is shown in Figure 2. It is parameterized by a set of variables, among which delay and magnitude are considered the most influential. These two are therefore selected for tuning and jointly denoted by  $\theta \in \mathbb{R}^2$ . As can be seen in Figure 1, the motor position  $y$  affects the inflation of the implanted balloon. This in turn affects the ICP, which is denoted by  $p \in \mathbb{R}$ . Given the periodicity of the cardiac

cycle, which is assumed to have a constant period length  $T \in \mathbb{N}$ , the relationship between motor position and ICP can be characterized as

$$\mathbf{p} = \Delta(\mathbf{y}), \quad (2)$$

where  $\Delta$  is an unknown function that maps the output sequence  $\mathbf{y} = \{y_0, \dots, y_{T-1}\}$  of the soft robotic actuator system to the ICP sequence  $\mathbf{p} = \{p_0, \dots, p_{T-1}\}$ , both being of period length  $T$ . Due to the highly nonlinear pressure-volume dynamics of the implanted balloon and the unpredictable physiological disturbances during in vivo application, the mapping described in (2) is difficult to model accurately.

The overarching goal of this work is to safely achieve a desired ICP waveform, which is defined through the mean pressure  $p_{\text{mean}} = \text{mean}(\mathbf{p})$  and the peak-to-peak amplitude  $p_{\text{amp}} = \max(\mathbf{p}) - \min(\mathbf{p})$  of the ICP sequence  $\mathbf{p}$  during a single cardiac cycle. For the specific example of replicating normal pressure hydrocephalus in vivo, as considered in Section IV, the peak-to-peak amplitude is to be increased to a reference amplitude  $p_{\text{amp}}^{\text{ref}}$  without raising the mean ICP from its baseline level  $p_{\text{mean}}^{\text{base}}$  at times when no actuation is performed. To achieve the desired ICP waveform modulation with the soft robotic actuator system, the problem is decomposed into two independent sub-problems, namely the reference tracking problem and the reference learning problem. The respective objectives of these two sub-problems are defined in detail as follows:

- 1) *Reference tracking:* Design a controller that steers the system output  $y$  as close as possible to the reference trajectory  $\mathbf{r}(\theta) = \{r_0, \dots, r_{T-1}\}$  while compensating for the model mismatch  $d$  and satisfying the system constraints  $x \in \mathbb{X}$  and  $u \in \mathbb{U}$ .
- 2) *Reference learning:* Find the optimal parameters  $\theta^*$  from a compact set of feasible parameters  $\Theta \subset \mathbb{R}^{n_\theta}$ , which yield a reference trajectory  $\mathbf{r}(\theta^*)$  that achieves the desired ICP waveform in terms of  $p_{\text{amp}}^{\text{ref}}$  and  $p_{\text{mean}}^{\text{base}}$ .

### III. METHODS

This section outlines the proposed methods for the soft robotic actuator system to safely achieve a desired ICP waveform modulation. Section III-A presents the MPC with disturbance observer for accurate and safe tracking of arbitrary motor reference trajectories. Section III-B presents the BO approach used for learning an optimal motor reference trajectory that yields the desired waveform modulation. The full learning-based control framework for the soft robotic actuator system is summarized in Algorithm 1.

#### A. Reference Tracking

This work employs an output reference tracking MPC that uses an augmented linear model with disturbance observer to achieve offset-free reference tracking [22–24]. The disturbance observer and MPC formulation are described in the following in detail.

*Disturbance observer:* To account for the model mismatch between the identified linear system model in (1) and the true system, the linear system model is augmented with the disturbance state  $d$ , which results in the following augmented system description

$$\begin{bmatrix} x(k+1) \\ d(k+1) \end{bmatrix} = \underbrace{\begin{bmatrix} A & B_d \\ 0 & I \end{bmatrix}}_{A_a} \begin{bmatrix} x(k) \\ d(k) \end{bmatrix} + \underbrace{\begin{bmatrix} B \\ 0 \end{bmatrix}}_{B_a} u(k), \quad (3a)$$

$$y(k) = \underbrace{\begin{bmatrix} C & C_d \end{bmatrix}}_{C_a} \begin{bmatrix} x(k) \\ d(k) \end{bmatrix}, \quad (3b)$$

where  $I$  describes an identity matrix of appropriate size, and  $A_a$ ,  $B_a$ , and  $C_a$  are the augmented state, input, and output matrix, respectively. For online estimation of the augmented state vector, the following Luenberger observer [25], [26] is designed

$$\begin{bmatrix} \hat{x}(k+1) \\ \hat{d}(k+1) \end{bmatrix} = A_a \begin{bmatrix} \hat{x}(k) \\ \hat{d}(k) \end{bmatrix} + B_a u(k) + \underbrace{\begin{bmatrix} L_x \\ L_d \end{bmatrix}}_L (y(k) - \hat{y}(k)), \quad (4a)$$

$$\hat{y}(k) = C_a \begin{bmatrix} \hat{x}(k) \\ \hat{d}(k) \end{bmatrix}, \quad (4b)$$

where the observer gain  $L$  is chosen via pole placement such that  $\tilde{A} - L\tilde{C}$  is Schur stable. The estimated disturbances of the full pulse sequence of length  $T$  are saved in the disturbance memory sequence  $\hat{\mathbf{d}} = \{\hat{d}_0, \dots, \hat{d}_{T-1}\}$  to be used by the MPC in the next period.

*Model predictive control:* To steer the system described in (1) toward its reference trajectory, an output reference tracking MPC with prediction horizon  $N$  is used. Given the reference trajectory  $\mathbf{r}(\theta) = \{r_0, \dots, r_{T-1}\}$ , the estimated disturbance sequence of the previous period  $\hat{\mathbf{d}}$  and the current state estimate  $\hat{x}(k)$  obtained from the observer in (4), the

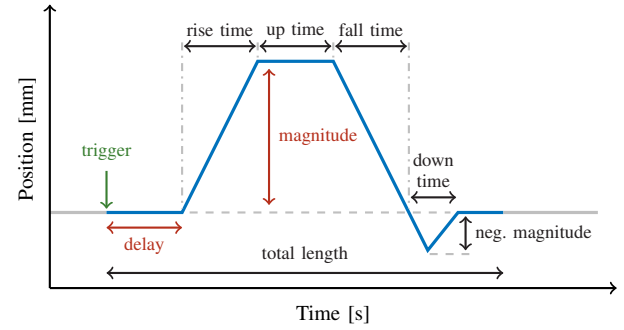


Fig. 2. Visualization of the periodically triggered and pulse-shaped reference trajectory for the motor position of the soft robotic actuator system. The delay and magnitude (red arrows) are tunable parameters that are determined via Bayesian optimization. The next pulse can only be triggered by the detection of an QRS complex in the electrocardiogram after the previous pulse has been completed. In between pulses, the motor is regulated to its baseline position (gray line).

MPC controller  $\pi_{\text{MPC}}$  computes at each time step  $k$  the input  $u(k)$  by solving the following optimization problem

$$\min_{\mathbf{x}, \mathbf{u}} \sum_{i=0}^{N-1} \|Cx_i + C_d \hat{d}(k+i-T) - r_{k+i}\|_2^2, \quad (5a)$$

$$\text{s.t. } \forall i = 0, \dots, N-1, \quad (5b)$$

$$x_{i+1} = Ax_i + Bu_i + B_d \hat{d}(k+i-T), \quad (5b)$$

$$(x_i, u_i) \in \mathbb{X} \times \mathbb{U}, \quad (5c)$$

$$x_0 = \hat{x}(k). \quad (5d)$$

In contrast to standard offset-free MPC formulations [22–24], we leverage the iterative nature of the problem by utilizing the disturbance estimates from the previous pulse sequence in the MPC prediction, similar to [27]. The considered singular output cost is applicable since the model  $(A, B, C)$  is flat (otherwise an input regularization should be added, see [28], [29]). Closed-loop stability can be ensured if the reference trajectory  $\mathbf{r}(\theta)$  is feasible and a sufficiently long prediction horizon  $N$  is utilized [28], [29].

#### B. Reference Learning

To achieve the desired ICP waveform modulation, the correct reference trajectory  $\mathbf{r}(\theta)$  for the MPC must be found. Since the mapping between the system's output sequence  $\mathbf{y}$  and the ICP sequence  $\mathbf{p}$  in (2) is unknown, a black-box optimization approach based on BO is chosen to learn the optimal motor position reference trajectory. BO has been widely applied in control, particularly for automatic controller tuning [30–32], motivating its use in this work for automatic tuning of the reference trajectory parameterization shown in Figure 2. Specifically, the aim of the proposed BO algorithm is to find the optimal parameter values  $\theta^*$  that minimize a cost function  $J(\theta)$ , which quantifies the deviation between the observed and desired ICP waveform characteristics. The cost function is evaluated over the full period of length  $T$  and defined as

$$J(\theta) = - \left( p_{\text{amp}} - p_{\text{amp}}^{\text{ref}} \right)^2 - \lambda \sum_{i=0}^{T-1} p_i^2. \quad (6)$$

---

**Algorithm 1** Offset-free MPC with Reference Learning

---

- 1: **Input:** Number of max iterations  $n_m$ , number of random samples  $n_r$ , number of evaluation periods per iteration  $n_p$ , number of time steps per period  $T$ , hyperparameter  $\beta$ , disturbance threshold  $\varepsilon$ , and feasible parameter set  $\Theta$
- 2: **Initialize:** GP prior  $J(\theta) \sim GP(\mu_0, \sigma_0)$ , dataset  $D_0$ , and sequence of disturbance estimates  $\hat{\mathbf{d}}$
- 3: **for**  $n = 1, \dots, n_m$  **do**
- 4:   **if**  $n \leq n_r$  **then**
- 5:      $\theta_n \leftarrow$  Sample parameters randomly from  $\Theta$
- 6:   **else**
- 7:      $\mu_{n-1}(\theta), \sigma_{n-1}(\theta) \leftarrow$  Update GP based on  $D_{1:n-1}$
- 8:      $\theta_n \leftarrow \arg \max_{\theta \in \Theta} \mu_{n-1}(\theta) + \beta \cdot \sigma_{n-1}(\theta)$
- 9:   **end if**
- 10:    $l \leftarrow 0$  Initialize evaluation period counter
- 11:   **while**  $l \leq n_p$  **do**
- 12:     **for**  $k = 0, \dots, T - 1$  **do**
- 13:        $y_k \leftarrow$  Take measurement
- 14:        $\hat{x}_k, \hat{d}_k \leftarrow$  Estimate state and disturbance
- 15:        $u_k \leftarrow$  Compute input using  $\pi_{\text{MPC}}(\hat{x}_k, \hat{\mathbf{d}}, \mathbf{r}(\theta_n))$
- 16:     **end for**
- 17:     **if**  $|\hat{d}_k - \hat{d}_k| \leq \varepsilon \forall k \in [0, T - 1]$  **then**
- 18:        $J_n^l \leftarrow$  Evaluate parameter cost of period  $l$
- 19:        $l \leftarrow l + 1$  Advance counter
- 20:     **end if**
- 21:      $\hat{\mathbf{d}} \leftarrow \hat{\mathbf{d}}'$  Update disturbance estimates
- 22:   **end while**
- 23:    $J_n \leftarrow$  Evaluate cost for  $\theta_n$  as average of  $n_p$  periods
- 24:    $D_{0:n} \leftarrow$  Update dataset with  $D_{0:n-1} \cup \{(\theta_n, J_n)\}$
- 25: **end for**
- 26: **Return:** optimal parameters  $\theta^*$

---

The first term penalizes the difference between the observed and desired peak-to-peak amplitude of the ICP, whereas the second term penalizes the energy of the ICP signal in order to prevent any increase in the mean ICP from the baseline value. The hyperparameter  $\lambda \geq 0$  trades off the two terms in the cost function. To reduce the variance in the cost evaluation, the parameter cost is computed as the average over a series of  $n_p$  measured periods. To filter out transient effects in the reference tracking performance caused by changes in the parameter setting  $\theta$ , measured periods are counted toward these  $n_p$  periods only after the difference between two consecutive estimates of the disturbance sequence  $\hat{\mathbf{d}}$  falls below a predefined threshold  $\varepsilon \in \mathbb{R}_{>0}$ .

In the proposed BO algorithm, a Gaussian process (GP) [33] with a squared-exponential kernel is employed to construct a probabilistic surrogate model of the cost function (6). The algorithm is initialized by uniformly sampling and evaluating  $n_r$  parameters from the feasible parameter set  $\Theta$ . In each of the subsequent iterations, indexed by  $n$ , a new candidate  $\theta_n$  is selected by maximizing an acquisition function based on the upper confidence bound [34]:

$$\theta_n = \arg \max_{\theta \in \Theta} \mu_{n-1}(\theta) + \beta \cdot \sigma_{n-1}(\theta), \quad (7)$$

where  $\mu_{n-1}(\theta)$  and  $\sigma_{n-1}(\theta)$  denote the posterior mean and standard deviation of the GP model at iteration  $n-1$ , conditioned on the dataset  $D_{1:n-1} = \{(\theta_1, J_1), \dots, (\theta_{n-1}, J_{n-1})\}$  of previous experiments and their corresponding costs. The hyperparameter  $\beta > 0$  regulates the trade-off between exploitation and exploration.

## IV. EXPERIMENTS

This section presents the experimental evaluation of the proposed learning-based control framework for the soft robotic actuator system. While Section IV-A evaluates the MPC tracking performance, Section IV-B evaluates the full framework's ICP waveform modulation performance. In both experiments, commercially available Fogarty balloon catheters with a maximum volume of 2.5 mL were used as the soft robotic end actuators.

### A. Reference Tracking

Accurate tracking of the actuator system's motor reference trajectory is essential for enabling precise ICP waveform modulation. Deviations from the desired trajectory can introduce unintended pressure fluctuations, potentially compromising the system's effectiveness. The first experiment is therefore dedicated to the evaluation of the motor position tracking performance of the proposed MPC scheme. To this end, the soft robotic actuator system shown in Figure 1 is first evaluated in standalone operation, i.e., without integration into the test bench. During the experiment, the system is tasked with following a reference trajectory similar to those reference trajectories used during the later application for ICP waveform modulation shown in Figure 2. The motor position is initialized at a baseline of 0.63 mm, just before the balloon inflation begins. The reference trajectory consists of pulses with a magnitude of 0.5 mm at 60 beats per minute (BPM). Three control approaches are compared:

- 1) PID controller
- 2) MPC without disturbance observer
- 3) MPC with disturbance observer (offset-free MPC)

For the MPC-based controllers, the system matrix  $A$  and input matrix  $B$  are identified from representative experimental data using the prediction error method [35]. Both MPC schemes use a prediction horizon of  $N = 15$ . For the Luenberger observer, the disturbance matrices are chosen as  $B_d = 0$  and  $C_d = 1$ , ensuring observability of the augmented system (3). The system's state constraints  $\mathbb{X}$  and input constraints  $\mathbb{U}$  are provided in Table I. The disturbance observer and MPC are implemented on a real-time embedded computer (MicroLabBox, dSpace, Paderborn, Germany) with Acados [36] and run at a frequency of 100 Hz.

The tracking performance of the three compared control approaches is illustrated in Figure 3. The PID controller exhibits significant phase lag and struggles to accurately follow the reference trajectory. In contrast, both MPC-based approaches effectively capture the pulse shape since they can use the preview of the reference trajectory. However, minor undershoots and overshoots following the rising and falling edges of the trajectory can be observed. Additionally, offsets

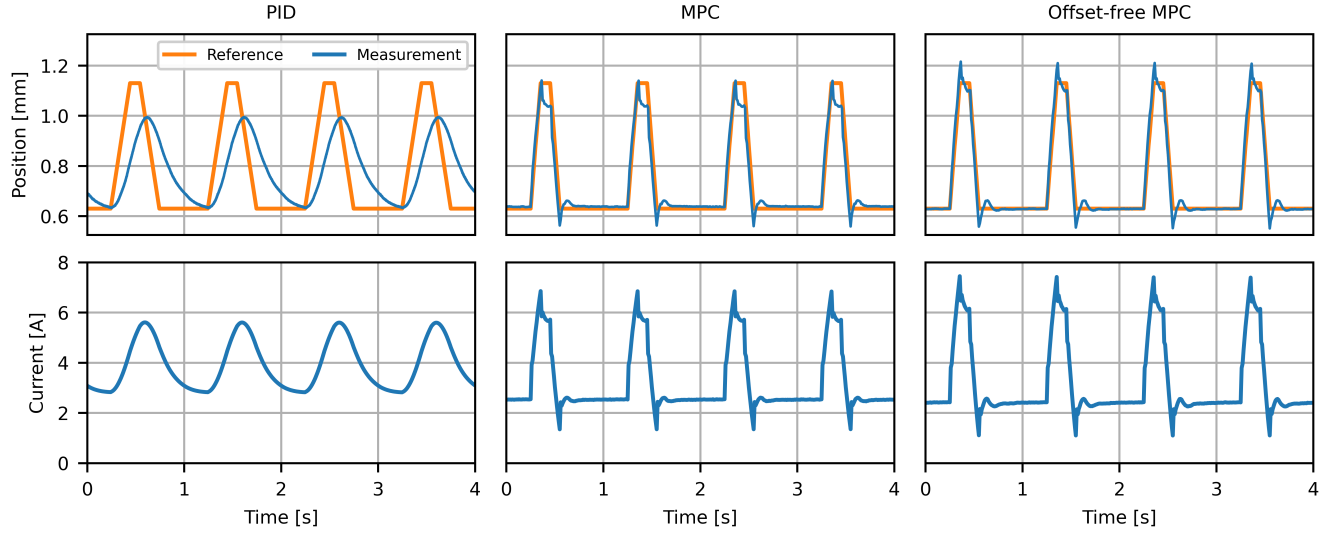


Fig. 3. Reference tracking experiment: Comparison of the baseline proportional-integral-derivative (PID) controller, the model predictive controller (MPC) without disturbance observer, and the MPC with disturbance observer (offset-free MPC). The upper panels show the motor position of the actuator system, whereas the lower panels show the motor current. All controllers were tested at 60 BPM using the same reference trajectory.

TABLE I  
STATE AND INPUT CONSTRAINTS OF THE SYSTEM

Constraint	Lower Limit	Upper Limit	Unit
<b>Motor Position</b>	0	2.6	mm
<b>Motor Velocity</b>	-100	+100	$\text{mm s}^{-1}$
<b>Motor Input</b>	-10	+10	A

TABLE II  
EXPERIMENTAL REFERENCE TRACKING RESULTS

Controller	NRMSE [%]	Max. Error [mm]
<b>PID</b>	32.3	0.316
<b>MPC</b>	8.0	0.119
<b>Offset-free MPC</b>	5.5	0.086

in the plateau regions are observed when using the MPC without disturbance observer. The MPC with disturbance observer achieves offset-free reference tracking, i.e., the controller accurately maintains the desired motor position without steady-state errors during segments with constant motor position reference.

To quantitatively assess tracking performance, the following two metrics are computed. First, the normalized root mean square error (NRMSE) is used to evaluate the average deviation from the reference trajectory while accounting for variations in trajectory magnitude. It is defined as

$$\text{NRMSE} [\%] = 100 * \frac{\sqrt{\frac{1}{M} \sum_{k=0}^{M-1} (r_k - y_k)^2}}{\max(\mathbf{r}_M) - \min(\mathbf{r}_M)}, \quad (8)$$

where  $\mathbf{r}_M = \{r_0, \dots, r_{M-1}\}$  and  $\mathbf{y}_M = \{y_0, \dots, y_{M-1}\}$  represent the reference and system output during the full test sequence of length  $M$ , respectively. Second, the maximum

absolute tracking error (MATE) is used to quantify the worst-case deviation between the motor position and its reference trajectory. It is formally defined as

$$\text{MATE} [\text{mm}] = \max(\text{abs}(\mathbf{r}_M - \mathbf{y}_M)). \quad (9)$$

The results for both metrics are summarized in Table II. Compared to the baseline PID controller, the MPC without a disturbance observer reduces the NRMSE by 75 % and the MATE by 62 %. The augmentation of the MPC with the disturbance observer further enhances tracking performance. Compared to the baseline PID controller, the offset-free MPC reduces the NRMSE by 83 % and the MATE by 73 %.

### B. Waveform Modulation

The second experiment is dedicated to evaluating the soft robotic actuator system's ICP waveform modulation capabilities when using the full learning-based control framework, i.e., the offset-free reference tracking MPC with BO-based reference learning. To this end, the experimental test setup as shown in Figure 1 was used and the balloon catheter inserted into the ventricle of the brain phantom. Two test scenarios were conducted, corresponding to constant heart rates of 60 BPM and 90 BPM. The mechatronic test bench was utilized to replicate a physiological ICP waveform of the respective heart rate with a mean pressure of 15 mmHg and a peak-to-peak amplitude of 1 mmHg [37] in vitro. In both test scenarios, the objective was to induce pathological ICP waveform patterns that are typically observed in normal pressure hydrocephalus [38]. Specifically, the peak-to-peak ICP amplitude should be doubled while avoiding any increase in mean ICP. During testing, the MPC with disturbance observer was utilized for tracking the actuator system's motor position reference trajectory. For reference learning, the BO algorithm used a total of  $n = 20$  iterations

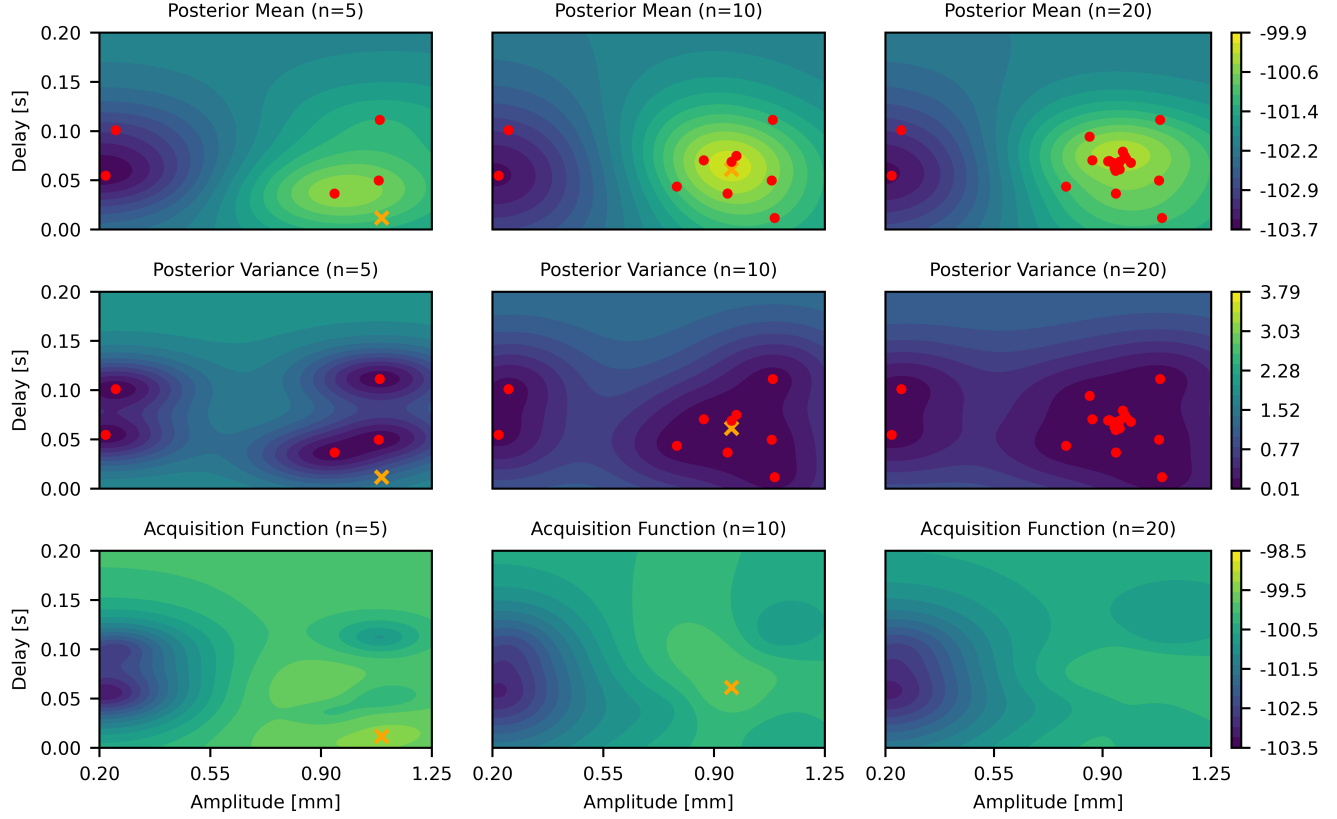


Fig. 4. Waveform modulation experiments at 90 BPM: Results of the Bayesian optimization (BO) algorithm used for tuning the delay and magnitude parameter of the controller's motor position reference trajectory. The top panels show the posterior mean of the Gaussian process (GP), the middle panels show the posterior variance of the GP, and the bottom panels show the acquisition function based on the upper confidence bound in (7). Red dots represent evaluated parameters, whereas orange crosses represent new parameter candidates computed by maximizing the acquisition function. The  $n = 5$  samples in the leftmost plots represent the randomly sampled parameters used for initialization of the BO algorithm.

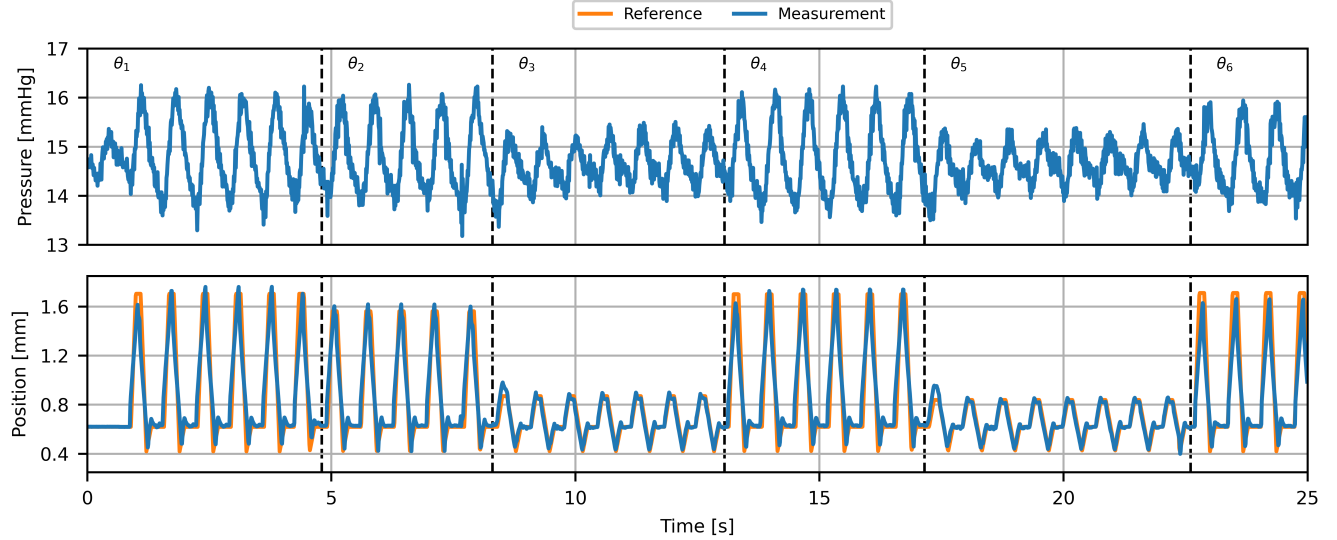


Fig. 5. Waveform modulation experiment at 90 BPM: Results of the actuation-based intracranial pressure (ICP) waveform modulation during the first six iterations of the Bayesian optimization (BO) algorithm used for automated reference learning. The upper panel shows the ICP inside the brain phantom of the test bench, whereas the lower panel shows the motor position of the soft robotic actuator system. Changes in the parameterization  $\theta$  of the reference trajectory, i.e., BO iterations, are highlighted by vertical dashed lines. A minimum of five cycles were performed per parameter setting.

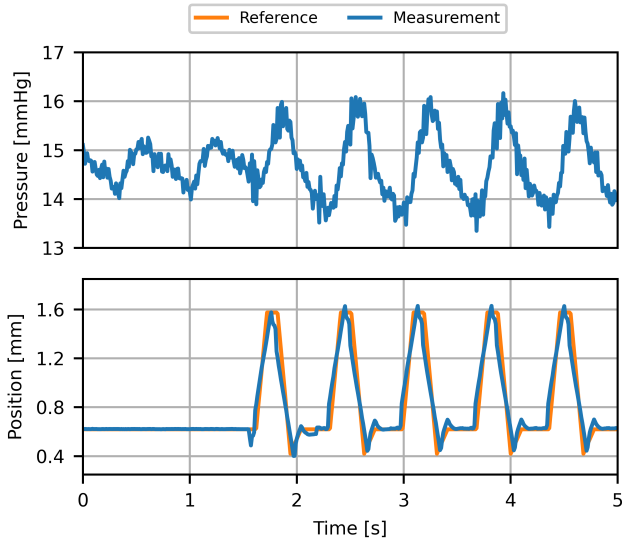


Fig. 6. Waveform modulation experiment at 90 BPM: Results of the actuation-based intracranial pressure (ICP) waveform modulation with the final parameter values resulting from the Bayesian optimization algorithm used for automated reference learning. The upper panel shows the ICP inside the brain phantom of the test bench, whereas the lower panel shows the motor position of the soft robotic actuator system. In the beginning, the actuation device is in a steady state and only the natural ICP waveforms as simulated by the test bench are visible in the phantom pressure. In the following, the soft robotic actuator system doubles the peak-to-peak amplitude of the ICP without significantly increasing the mean pressure.

to tune the delay and amplitude parameters of the reference trajectory. The initial  $n_r = 5$  parameter were sampled randomly from the feasible parameter set  $\Theta$ . The delay was allowed to range from 0s to 0.2s, whereas the magnitude was allowed to range from 0.2mm to 1.25mm. While the BO algorithm is implemented on the actuator system's host PC using GPytorch [39], the data acquisition and processing is conducted on the MicroLabBox. For data transfer between the host PC and the MicroLabBox, serial communication with the RS232 standard is established using the PySerial library and the dSpace RTI library.

The quantitative results for both test scenarios are presented in Table III. With amplification factors of 1.885 in the 60 BPM test scenario and 2.099 in the 90 BPM test scenario, the desired doubling of the amplitude was closely achieved. The relative increases in the respective mean ICP of 0.55 % and 1.28 % are negligibly small, as desired. For the 90 BPM test scenario, detailed results of the BO algorithm are shown in Figure 4. During this tuning process, the reference trajectory is iteratively updated and accurately tracked by the MPC, leading to progressively improved ICP modulation. Reference tracking and actuation-based ICP waveform modulation corresponding to the first six iterations of the BO algorithm are shown in Figure 5. Improvements are particularly evident when comparing settings 5 and 6 in Figure 5, where changes in the learned trajectory directly translate into significant better ICP waveform modulation. The ICP waveform modulation using the final parameters resulting from the BO algorithm is shown in Figure 6. Instead

TABLE III  
EXPERIMENTAL WAVEFORM MODULATION RESULTS

Experiment	Criteria	Results
60 BPM	Peak-to-peak ICP - baseline	0.903 mmHg
	Peak-to-peak ICP - actuated	1.704 mmHg
	Amplification factor	1.885
	Mean ICP - baseline	15.197 mmHg
	Max absolute mean ICP increase	0.084 mmHg
	Max relative mean ICP increase	0.550 %
90 BPM	Optimal Reference Delay	0.060 s
	Optimal Reference Amplitude	1.066 mm
	Peak-to-peak ICP - baseline	0.991 mmHg
	Peak-to-peak ICP - actuated	2.080 mmHg
	Amplification factor	2.099
	Mean ICP - baseline	14.668 mmHg
	Max absolute mean ICP increase	0.188 mmHg
	Max relative mean ICP increase	1.280 %
	Optimal Reference Delay	0.069 s
	Optimal Reference Amplitude	0.955 mm

of relying on time-consuming and error-prone hand-tuning, the desired ICP waveform modulation is achieved in an automated and safe manner within less than 2 min.

## V. CONCLUSION

This work introduces a learning-based model predictive control (MPC) framework to safely achieve a desired intracranial pressure (ICP) waveform modulation with a soft robotic actuator system. For accurate and constraint-aware tracking of the system's motor position reference trajectory, the framework combines a tracking MPC with a disturbance observer that exploits the periodic operation of the system. As the exact influence of the motor position on the ICP cannot be modeled precisely, the framework employs a Bayesian optimization algorithm for online learning of the optimal motor position reference trajectory that yields the desired ICP waveform modulation. Experimental validation using a mechatronic test bench replicating physiological ICP waveform patterns demonstrates that the soft robotic actuator system efficiently and safely learns how to double the ICP peak-to-peak amplitude without significantly raising the mean ICP, thereby inducing pathological waveform patterns observed in normal pressure hydrocephalus. The presented technical contributions are of high significance in neurological research and clinical practice, as they not only enhance the safety of in vivo interventions and eliminate time-consuming and error-prone hand-tuning efforts, but could also improve experimental outcomes through more precise ICP waveform modulation capabilities. The introduced learning-based MPC framework may make the soft robotic actuator system a valuable tool for studying cerebrospinal fluid dynamics and related neurological conditions under controlled experimental conditions, as exemplified by the presented application in hydrocephalus research.

## ACKNOWLEDGMENT

The authors thank Prof. Dr. Steffen Leonhardt and Dr. Marian Walter from RWTH Aachen University for providing the mechatronic test bench.

## REFERENCES

- [1] A. Aschoff, P. Kremer, B. Hashemi, and S. Kunze, "The scientific history of hydrocephalus and its treatment," *Neurosurgical Review*, 1999.
- [2] M. A. Williams and J. Malm, "Diagnosis and treatment of idiopathic normal pressure hydrocephalus," *Continuum*, 2016.
- [3] F. Flürenbrock, L. Korn, D. Schulte, A. Podgoršak, J. Chomarat, J. Hug, T. Hungerland, C. Holzer, D. Iselin, L. Krebs, R. Weiss, M. F. Oertel, L. Stieglitz, M. Weisskopf, M. Meboldt, M. N. Zeilinger, and M. Schmid Daners, "VIEnshunt: towards a ventricular intelligent and electromechanical shunt for hydrocephalus therapy," *Fluids and Barriers of the CNS*, 2025.
- [4] K. B. Evensen and P. K. Eide, "Measuring intracranial pressure by invasive, less invasive or non-invasive means: Limitations and avenues for improvement," *Fluids and Barriers of the CNS*, 2020.
- [5] L. M. Green, T. Wallis, M. U. Schuhmann, and M. Jaeger, "Intracranial pressure waveform characteristics in idiopathic normal pressure hydrocephalus and late-onset idiopathic aqueductal stenosis," *Fluids and Barriers of the CNS*, 2021.
- [6] R. Mancinelli and V. E. Pettorossi, "A Device for Increasing the Amplitude of the Pulse Pressure of Cerebrospinal Fluid," *Physiology & Behavior*, 1976.
- [7] C. Di Rocco, V. E. Pettorossi, M. Caldarelli, R. Mancinelli, and F. Velardi, "Experimental hydrocephalus following mechanical increment of intraventricular pulse pressure," *Experientia*, 1977.
- [8] C. Di Rocco, V. E. Pettorossi, M. Caldarelli, R. Mancinelli, and F. Velardi, "Communicating hydrocephalus induced by mechanically increased amplitude of the intraventricular cerebrospinal fluid pressure: experimental studies," *Experimental Neurology*, 1978.
- [9] V. E. Pettorossi, C. Di Rocco, R. Mancinelli, M. Caldarelli, and F. Velardi, "Communicating hydrocephalus induced by mechanically increased amplitude of the intraventricular cerebrospinal fluid pulse pressure: Rationale and method," *Experimental Neurology*, 1978.
- [10] M. G. Luciano, S. M. Dombrowski, S. Qvarlander, S. El-Khoury, J. Yang, S. Thyagaraj, and F. Loth, "Novel method for dynamic control of intracranial pressure," *Journal of Neurosurgery*, 2017.
- [11] M. G. Luciano, S. M. Dombrowski, S. El-Khoury, J. Yang, S. Thyagaraj, S. Qvarlander, S. Khalid, I. Suk, A. Manbachi, and F. Loth, "Epidural oscillating cardiac-gated intracranial implant modulates cerebral blood flow," *Neurosurgery*, 2020.
- [12] S. Qvarlander, S. M. Dombrowski, D. Biswas, S. Thyagaraj, F. Loth, J. Yang, and M. G. Luciano, "Modifying the ICP pulse wave: effects on parenchymal blood flow pulsatility," *Journal of Applied Physiology*, 2023.
- [13] O. Doron, T. Or, L. Battino, G. Rosenthal, and O. Barnea, "Cerebral blood flow augmentation using a cardiac-gated intracranial pulsating balloon pump in a swine model of elevated ICP," *Journal of Neurosurgery*, 2020.
- [14] O. Doron, O. Barnea, N. Stocchetti, T. Or, E. Nossek, and G. Rosenthal, "Cardiac-gated intracranial elastance in a swine model of raised intracranial pressure: A novel method to assess intracranial pressure-volume dynamics," *Journal of Neurosurgery*, 2021.
- [15] O. Doron, Y. Zadka, G. Rosenthal, and O. Barnea, "Intracranial Pulsating Balloon-Based Cardiac-Gated ICP Modulation Impact on Brain Oxygenation: A Proof-of-Concept Study in a Swine Model," *Neurocritical Care*, 2022.
- [16] F. Flürenbrock, L. Rosalia, A. Podgorsak, K. Sapozhnikov, N. E. Trimmel, M. Weisskopf, M. F. Oertel, E. Roche, M. N. Zeilinger, L. Korn, and M. Schmid Daners, "A Soft Robotic Actuator System for In Vivo Modeling of Normal Pressure Hydrocephalus," *IEEE Transactions on Biomedical Engineering*, 2024.
- [17] A. A. Linninger, K. Tangen, C.-Y. Hsu, and D. Frim, "Cerebrospinal Fluid Mechanics and Its Coupling to Cerebrovascular Dynamics," *Annual Review of Fluid Mechanics*, 2016.
- [18] L. S. Fridericia, "The duration of systole in an electrocardiogram in normal humans and in patients with heart disease," *Annals of Noninvasive Electrocardiology*, 2003.
- [19] J. B. Rawlings, D. Q. Mayne, and M. M. Diehl, *Model Predictive Control: Theory, Computation, and Design*. Nob Hill Publishing, 2 ed., 2017.
- [20] B. Shahriari, K. Swersky, Z. Wang, R. P. Adams, and N. De Freitas, "Taking the human out of the loop: A review of Bayesian optimization," *Proceedings of the IEEE*, 2016.
- [21] C. Castelar Wemers, F. Flürenbrock, B. Maurer, A. Benninghaus, K. Radermacher, and S. Leonhardt, "A mechatronic test-bench to investigate the impact of ventricular pulsation in hydrocephalus," *Biomedical Signal Processing and Control*, 2022.
- [22] K. R. Muske and T. A. Badgwell, "Disturbance modeling for offset-free linear model predictive control," *Journal of Process Control*, 2002.
- [23] G. Pannocchia and J. B. Rawlings, "Disturbance models for offset-free model-predictive control," *AIChE Journal*, 2003.
- [24] U. Maeder, F. Borrelli, and M. Morari, "Linear offset-free model predictive control," *Automatica*, 2009.
- [25] D. G. Luenberger, "Observers for Multivariable Systems," *IEEE Transactions on Automatic Control*, 1966.
- [26] G. Pannocchia, M. Gabiccini, and A. Artoni, "Offset-free MPC explained: Novelties, subtleties, and applications," *IFAC-PapersOnLine*, 2015.
- [27] L. Pabon, J. Köhler, J. I. Alora, P. B. Eberhard, A. Carron, M. N. Zeilinger, and M. Pavone, "Perfecting Periodic Trajectory Tracking: Model Predictive Control with a Periodic Observer," *International Conference on Intelligent Robots and Systems (IROS)*, 2024.
- [28] J. Köhler, M. A. Müller, and F. Allgöwer, "Analysis and design of model predictive control frameworks for dynamic operation-An overview," *Annual Reviews in Control*, 2024.
- [29] J. Köhler, M. A. Müller, and F. Allgöwer, "Constrained nonlinear output regulation using model predictive control," *IEEE Transactions on Automatic Control*, 2022.
- [30] F. Berkenkamp, A. P. Schoellig, and A. Krause, "Safe controller optimization for quadrotors with Gaussian processes," *International Conference on Robotics and Automation (ICRA)*, 2016.
- [31] A. Marco, P. Henning, J. Bohg, S. Schaal, and S. Trimpe, "Automatic LQR Tuning Based on Gaussian Process Global Optimization," *International Conference on Robotics and Automation (ICRA)*, 2016.
- [32] F. Sorourifar, G. Makrygirgios, A. Mesbah, and J. A. Paulson, "A Data-Driven Automatic Tuning Method for MPC under Uncertainty using Constrained Bayesian Optimization," *IFAC-PapersOnLine*, 2021.
- [33] C. E. Rasmussen and C. K. I. Williams, *Gaussian processes for machine learning*. MIT Press, 2006.
- [34] N. Srinivas, A. Krause, and M. Seeger, "Gaussian Process Optimization in the Bandit Setting: No Regret and Experimental Design," *International Conference on Machine Learning (ICML)*, 2010.
- [35] L. Ljung, *System identification: theory for the user*. Prentice Hall, 2nd ed., 1999.
- [36] R. Verschueren, G. Frison, D. Kouzoupis, J. Frey, N. v. Duijkeren, A. Zanelli, B. Novoselnik, T. Albin, R. Quirynen, and M. Diehl, "acados—a modular open-source framework for fast embedded optimal control," *Mathematical Programming Computation*, 2022.
- [37] S. Qvarlander, J. Malm, and A. Eklund, "The pulsatility curve—the relationship between mean intracranial pressure and pulsation amplitude," *Physiological Measurement*, 2010.
- [38] D. Shprecher, J. Schwalb, and R. Kurlan, "Normal Pressure Hydrocephalus: Diagnosis and Treatment," *Current Neurology and Neuroscience Reports*, 2008.
- [39] J. R. Gardner, G. Pleiss, D. Bindel, K. Q. Weinberger, and A. G. Wilson, "GPyTorch: Blackbox matrix-matrix gaussian process inference with GPU acceleration," *Conference on Neural Information Processing Systems (NeurIPS)*, 2018.